Aggressive Cholesterol Lowering Normalizes Atherosclerosis Regression in *Jak2*^{V617F} Clonal Hematopoiesis

Brian D. Hardaway (MPhil)[1], Trevor P. Fidler (PhD)[2], Mojdeh Tavallaie (PharmD-PhD)[1], Kleopatra Avrampou (PhD)[1], Cheng-Chieh Hsu (PhD)[1], Sandra Schiavone (MA)[1], Tong Xiao (MS)[1], Nan Wang (PhD)[1*], Alan R. Tall (MD)[1*]

[1]Division of Molecular Medicine, Department of Medicine, Columbia University Irving Medical Center, New York, NY, USA.

[2]Cardiovascular Research Institute, University of California San Francisco, San Francisco, CA, USA.

Short Title: Atherosclerosis Regression in *Jak2*^{V617F} CH

[*]These authors contributed equally to this work.

Correspondence to:

Alan R. Tall: art1@cumc.columbia.edu

Abstract

Background - Clonal hematopoiesis (CH) has emerged as an important risk factor for atherosclerotic cardiovascular disease (ACVD). Mouse studies have established a causal role of CH in atherosclerosis progression and have defined macrophage inflammatory responses as a key underlying mechanism. We undertook the present study to assess the hypothesis that ongoing inflammation would impede atherosclerosis regression in *Jak2*^{V617F} (*Jak2*^{VF}) CH mice.

Methods and Results - Chimeric *Jak2*$^{VF/WT}$ or control *WT/WT* bone marrow was transplanted into *Ldlr*$^{-/-}$ mice and, following 13-16 weeks of Western diet-induced atherosclerosis progression, cholesterol was lowered either moderately (to 200-300 mg/dl) or markedly (to 100 mg/dl). With moderate cholesterol lowering there was impaired regression in *Jak2*^{VF} CH mice compared to controls. However, with marked cholesterol lowering, regression was similar in *Jak2*^{VF} CH and control mice.

Two mechanisms of low-density lipoprotein (LDL) lowering-induced suppression of inflammation in plaques were implicated: 1) reversal of increased proliferation, DNA damage and Absent in Melanoma 2 (AIM2) inflammasome activation specifically in *Jak2*^{VF} macrophages and 2) markedly increased macrophage triggering receptor expressed on myeloid cells 2 (TREM2), c-myc expressing macrophages in both *Jak2*^{VF} and control mice.

Conclusions - Aggressive LDL lowering reverses inflammasome activation and induces pro-resolving changes in macrophages in *Jak2*^{VF} CH, halting atherosclerosis progression and promoting features of plaque stabilization. These findings suggest that aggressive LDL cholesterol lowering could effectively reverse ACVD risk in individuals with *JAK2*^{VF} clonal hematopoiesis.

36 **Translational Perspective**

37 Clonal hematopoiesis increases the risk of atherosclerotic cardiovascular disease. Amongst
38 mutations associated with clonal hematopoiesis, *Jak2*^{V617F} confers the greatest increased risk of
39 atherosclerotic cardiovascular disease. Our findings demonstrate that aggressive LDL lowering
40 normalizes atherosclerosis regression in *Jak2*^{V617F} clonal hematopoiesis by reversing
41 inflammasome activation and inducing pro-resolving changes in macrophages. These changes
42 lead to increased features of plaque stability, including decreased macrophage burden, increased
43 collagen, and improved efferocytosis. These results suggest that aggressive LDL-C lowering in
44 *Jak2*^{V617F} clonal hematopoiesis patients would mitigate the increased atherosclerotic
45 cardiovascular disease risk.

46 **1. Introduction**

47 Despite therapeutic advances, ACVD remains the leading cause of death in the developed
48 world.[1] Although inflammation plays a key role in atherosclerosis progression, cholesterol
49 accumulation remains a prerequisite for lesion development, and LDL lowering has consistently
50 shown a benefit in many clinical trials.[2-4]

51 The role of inflammation in increasing ACVD risk has also now been well established. The
52 LoDoCo 2 trial found that the risk of cardiovascular events was significantly lower in patients
53 with chronic coronary disease who were given 0.5 mg of colchicine daily.[5] Based on these and
54 other results, the FDA approved the use of low dose colchicine as the first anti-inflammatory
55 drug for heart disease.[6] The CANTOS trial involving the use of interleukin-1β (IL-1β) antibodies
56 showed reduced cardiovascular events in high-risk patients with mean LDL cholesterol levels of
57 81 mg/dl - 84 mg/dl and a high-sensitivity C-reactive protein (hs-CRP) level of at least 2 mg/L.

58 However, there was a small increase in fatal infections, and the FDA did not approve this
59 treatment for marketing.[7] Many observations suggest that hypercholesterolemia is linked to
60 inflammatory risk. For example, statins lower hs-CRP levels[8] and preclinical studies have shown
61 that cholesterol accumulation in plaque macrophages promotes inflammasome activation.[9-12]
62 However, the mechanisms linking hypercholesterolemia, macrophage cholesterol accumulation
63 and inflammation remain incompletely understood, especially in the clinically important context
64 of atherosclerosis regression induced by LDL lowering.[13-19]

65 Clonal hematopoiesis (CH) arises from somatic mutations in hematopoietic stem cells (HSC) that
66 confer a selective advantage and lead to clonal expansion of blood cells. CH commonly arises
67 from mutations in genes that mediate epigenetic modifications or cytokine signaling.[20,21]
68 Amongst CH mutations, *Jak2*^{VF}, which increases signaling by hematopoietic cytokines, confers
69 the greatest risk of ACVD.[22-24] Moreover, *JAK2*^{VF} has been detected in 3-4% of a general
70 European population,[25] and increases thrombotic risk and coronary artery plaque erosion even at
71 low variable allele frequency().[26,27,28] We showed in a hypercholesterolemic mouse model that
72 *Jak2*^{VF} CH exacerbates atherosclerosis via AIM2 inflammasome activation in mice[29] with genetic
73 studies suggesting a similar role in humans.[30] The AIM2 inflammasome is activated by double
74 stranded DNA fragments in the cytosol.[31] We proposed two potential mechanisms of DNA
75 damage underlying AIM2 inflammasome activation in *Jak2*^{VF} CH: increased proliferation of
76 *Jak2*^{VF} macrophages leading to DNA replication stress or increased mitochondrial glycolytic
77 metabolism, reactive oxygen species (ROS) formation and oxidative DNA damage. Based on
78 these findings, we hypothesized that LDL lowering-induced atherosclerosis regression would be
79 impaired in *Jak2*^{VF} CH mice due to persistence of the underlying mechanisms promoting
80 inflammasome activation. Contrary to our hypothesis, we found that cholesterol lowering

81 reversed inflammasome associated changes in *Jak2*^{VF} macrophages and that marked cholesterol
82 lowering induced regression similar to control mice. These studies suggest the importance of
83 rigorous control of LDL cholesterol levels in individuals with *JAK2*^{VF} clonal hematopoiesis.

84 **2. Methods**

85 Several experimental procedures were performed as previously described[16,29]

86 **2.1 Mice**

87 All mice used for these studies were male and on a C57BL/6J background. Mice were housed in
88 a pathogen-free facility under standard conditions of temperature (23 °C) with a 12-hour light-
89 dark with ad libitum food and water access. Cages and water were changed every 7-14 days. All
90 mouse experiments were approved by the Institutional Animal Care and Use Committee of
91 Columbia University under protocol number AABG0561, and were conducted in accordance
92 with NIH guidelines and the Guide for the Care and Use of Laboratory Animals. Mice
93 heterozygous for the *Jak2*^{VF} conditional knock-in allele were generated as previously
94 described.[32] *Jak2*^{VF} mice were then crossed to *Mx1-Cre* (The Jackson Laboratory, B6.Cg-
95 Tg(*Mx1-Cre*)1*Cgn*/J (003556) or *Scl-Cre* (The Jackson Laboratory, C57BL/6-Tg(Tal1-
96 cre/ERT)42-056Jrg/J (037466) to generate *Mx1-CreJak2*^{VF} and *Scl-CreJak2*^{VF} mice respectively.
97 *Scl-Cre-Jak2*^{VF} mice were then crossed with ZsGreen reporter mice (The Jackson Laboratory,
98 B6.Cg-Gt(ROSA)26Sor$^{tm6(CAG-ZsGreen1)Hze}$/J (Ai6(RCL-ZsGreen) (007906) to generate *Scl-*
99 *CreJak2*^{VF}*ZsGreen* mice. *Ldlr*$^{-/-}$ recipient mice for the *Mx1-CreJak2*^{VF} moderate cholesterol
100 lowering model that included *Myh11-Cre*^{ERT2} and *ZsGreen* alleles from a previous lineage-tracing
101 study were obtained from a collaborator and have been previously described.[33] However, these
102 alleles were not relevant to the experimental outcomes assessed and were not analyzed. Half of

103 the recipients were *Ldlr*$^{-/-}$ *Myh-11-CreZsGreen* while the other half either lacked the *ZsGreen*
104 allele or both the *ZsGreen* allele and the *Myh11-Cre*. For the *Mx1-CreJak2*^{VF} and *Scl-CreJak2*^{VF}
105 aggressive cholesterol lowering studies, *Ldlr*$^{-/-}$ recipient mice were purchased from The Jackson
106 Laboratory (B6.129S7-*Ldlr*tm1Her/J (002207)). Littermate control mice for studies involving
107 *Mx1-CreJak2*^{VF} mice contained either an allele with *Mx1-Cre* or the *Jak2*^{VF} transgene, but not
108 both. Littermate control mice for studies involving *Scl-CreJak2*^{VF}*ZsGreen* mice contained the
109 alleles for *Scl-Cre* and *ZsGreen* but not the *Jak2*^{VF} transgene.

110 **2.2 Bone Marrow Transplantation**

111 Bone marrow transplantations (BMT) were conducted as previously described with the following
112 exceptions.[10] For the *Mx1-CreJak2*^{VF} moderate cholesterol lowering study, donor mice were 8-12
113 weeks old while recipients were 11-14 weeks old. For the *Mx1-CreJak2*^{VF} effective cholesterol
114 lowering study, donor mice were 7-16 weeks old while recipients were 7 weeks old. For the *Scl-*
115 *CreJak2*^{VF} study, donor mice were 6-12 weeks old while recipients were 8 weeks old. For the
116 *Mx1-CreJak2*^{VF} moderate cholesterol lowering study, recipients were lethally irradiated once
117 with 10.5 Gy from a cesium gamma source. Due to decommissioning of the cesium gamma
118 source, recipients from the *Mx1-CreJak2*^{VF} and *Scl-CreJak2*^{VF} effective cholesterol lowering
119 studies were irradiated with 10.5 Gy using a Multirad 350 X-ray Irradiator from Precision X-
120 Ray. Within 24 hours of irradiation, bone marrow was isolated from donors with the indicated
121 genotypes. Total bone marrow cell number was quantified using an iN CYTO C-Chip
122 hemocytometer (DHC-N01) according to the manufacturer instructions. Irradiated mice were
123 randomized to treatment groups, anesthetized with isoflurane before receiving 3 x 10^6 total bone
124 marrow cells via intravenous (i.v.) injection at a total final volume of 100 µl. For the *Mx1-*
125 *CreJak2*^{VF} studies, recipients received either 6 x 10^5 *CD45.1Mx1-CreJak2*$^{VF/WT}$ or 6 x 10^5

126 *CD45.1* control bone marrow cells (20%) combined with 2.4 x 10^6 *CD45.2Jak2*$^{WT/WT}$ cells (80%).
127 For the *Scl-CreJak2*^{VF} study, recipients received either 6 x 10^5 *CD45.1CD45.2Scl-*
128 *CreJak2*$^{VF/WT}$*ZsGreen* or 6 x 10^5 *CD45.1CD45.2Scl-CreJak2*$^{WT/WT}$*ZsGreen* bone marrow cells
129 (20%) combined with 2.4 x 10^6 *CD45.1Jak2*$^{WT/WT}$ cells (80%). For the *Mx1-CreJak2*^{VF} studies,
130 mice were allowed to recover for four weeks after BMT before being injected intraperitonially
131 (i.p.) with 50 µg/mouse/day polyinosinic:polycytidylic acid (pIpC) two times, 48 hours apart.

132 **2.3 Atherosclerosis Studies**

133 For the *Mx1-CreJak2*^{VF} studies, power analysis using GPower3.1 indicated that with a total
134 sample size of 80 (n = 20 per group), the study had 80% power to detect an effect size of f = 0.32
135 at $\alpha = 0.05$, using two-way analysis of variance (ANOVA) across two genotypes and two
136 treatments. For the *Scl-CreJak2*^{VF} study, power analysis using GPower3.1 indicated that with a
137 total sample size of 80 (n = 16 per group), the study had 80% power to detect an effect size of f =
138 0.40 at $\alpha = 0.05$, using one-way ANOVA across five groups. Four weeks after BMT. *Ldlr*$^{-/-}$
139 recipient mice were fed a western diet (ENVIGO, cat. no. TD.88137) for the indicated times. For
140 the final 10 days of the western diet period of the *Scl-CreJak2*^{VF} study, mice were switched to a
141 western diet containing tamoxifen at 500 mg/kg by weight (ENVIGO, cat. no. TD130889). To
142 induce LDL lowering in the *Mx1-CreJak2*^{VF} study of Figure 1A, mice were administered 2 x 10^{11}
143 viral particles per mouse in 200 µl of 1X PBS via tail vein injection of an hDAD-*hLDLr* viral
144 vector (Gene Vector Core Laboratory at the Baylor College of Medicine) and switched to chow
145 diet. To induce LDL lowering in the *Mx1-CreJak2*^{VF} study of Figure 4A and the *Scl-CreJak2*^{VF}
146 study of Figure 6A, mice were administered 2.5 x 10^{11} genome copies per mouse in 100 µl of 1X
147 PBS via tail vein injection of an AAV8-TBG-*mLdlr* vector (AAV-263355, Vector Biolabs) and
148 switched to chow diet. Mice were anesthetized using 5% isoflurane via inhalation at a flow rate

149 of approximately 3L/min oxygen using a calibrated vaporizer. Anesthetic depth was assessed
150 continuously using respiratory rate monitoring and the toe-pinch reflex. Isoflurane was
151 administered acutely during procedures requiring anesthesia, including blood collection and
152 euthanasia. Blood collection was performed via retro-orbital sinus for plasma, complete blood
153 counts, and flow cytometric analysis at the indicated timepoints. For euthanasia, mice were first
154 rendered deeply unconscious with isoflurane, after which cervical dislocation was performed as a
155 secondary method to ensure death, in accordance with AVMA guidelines. Following euthanasia,
156 aortic roots were collected and fixed with 4% paraformaldehyde (PFA) (Electron Microscopy
157 Sciences 15710; 16% PFA diluted 1:4 in 1.33X PBS) for 24 hours at 4 $^{\circ}$C , then embedded in
158 paraffin.

159 **2.4 Histological Analysis**

160 Lesion area and necrotic core area were quantified as previously described.[22,29] Researchers
161 blinded to genotype sectioned paraffin-embedded aortic root lesions at similar points between
162 mice over a 150 µm span for a total of 50 sections spaced 3 µm apart with 2 sections per slide on
163 25 slides. Six total slides spaced 30 µm apart (slides 1,5,10,15,20,25) were then stained with
164 hematoxylin & eosin (H&E) (Sigma MHS32-1L; Abcam ab246824) and imaged with an
165 Olympus DP27 camera attached to an Olympus CX43 biological microscope set to the 10X
166 objective using Olympus cellSens Entry 3.1 software. Lesion area was then quantified in a
167 blinded fashion and the average of the six slides was used to determine lesion area. The Necrotic
168 core area was similarly quantified in a blinded fashion using the same six H&E sections.
169 Collagen was stained using the Polysciences Picrosirius Red Stain Kit (cat. no. 24901) according
170 to the manufacturer's instructions. The same slide between mice was stained and the collagen
171 quantified by applying a consistent color threshold to calculate the collagen-positive area as a

172 percentage of total lesion area. Picrosirius red was imaged via the same system used for H&E
173 imaging. All lesion analysis was conducted using FIJI software.

174 **2.5 Immunofluorescence**

175 Identical slides of aortic roots between mice were baked in a dry incubator at 60 °C for 30
176 minutes and then deparaffinized in Histo-clear (National Diagnostics HS-200/50-899-90147)
177 three times for 10 minutes. Histo-clear was removed by 20 shakes in 100% ethanol twice
178 followed by 20 shakes in Histoprep Reagent Alcohol (fisher HC-600-1GAL) before being
179 washed in tap water 7 times. Antigen retrieval was performed by placing slides either in citric
180 acid-based antigen retrieval solution (Vector Laboratories, H3300) or tris-based antigen retrieval
181 solution (Vector Laboratories, H3301) and pressure cooking for 15 minutes with a 5-minute
182 natural release in an Instant Pot IP-LUX pressure cooker. Citric acid-based antigen retrieval was
183 performed for all antibodies except for the antibody against cleaved GasD. After pressure
184 cooking, slides were cooled for 10 minutes and then washed 3 times for 5 minutes in 1X
185 phosphate buffered saline (PBS) (Boston Bioproducts BM-220; diluted 1:10). Hydrophobic
186 circles were drawn using a liquid blocker pen (Sigma Z377821). For antibodies sourced from
187 mice, mouse on mouse blocking was performed by incubating sections in 10% goat serum
188 (ThermoFisher 10000C) in 1X PBS (Corning 21-040-CM) with 1 drop of mouse-on-mouse block
189 per 1.25ml of solution (Vector Laboratories NC9290646) for 1 hour at room temperature in a
190 humidified chamber. Slides were then washed in 1X PBS containing tween 20 (Fisher BP337-
191 500) at a concentration of 0.01% (PBS-T) twice for 5 minutes and then in 1X PBS once for 5
192 minutes. For antibodies not sourced from mice, sections were blocked by incubating in Normal
193 Serum Block (Biolegend 927503) for 1 hour at room temperature in a humidified chamber.
194 Following blocking, sections were incubated with the following primary antibodies at the

195 indicated dilutions or concentrations overnight at 4 °C in a humidified chamber: AIM2 (Abcam,
196 ab119791, 1:250), 8-hydroxydeoxyGuanosine (Abcam, ab183395, 1:100), Cleaved GasD (Cell
197 Signaling, 10137, 10µg/ml), c-myc (Cell Signaling, 5605, 5.76 µg/ml), Ki67 (Abcam, ab15580,
198 9 µg/ml), MAC2 conjugated to Alexa Fluor 488 (Cedarlane, CL8942AF4, 1 µg/ml), MAC2
199 (Cedarlane, CL8942AP, 1 µg/ml), MerTK (R&D, BAF591, 2 µg/ml), pγH2AX (Cell Signaling,
200 9718, 0.74 µg/ml), ZsGreen (ThermoFisher, TA180002, 10 µg/ml), TREM2 (Denali, 4D9
201 DC1847, 1:100). The following IgG antibodies were used as negative controls for primary
202 antibodies sourced from the same species at the same concentration: Mouse IgG (ChromPure,
203 015-000-003), Rabbit IgG (Abcam, ab172730), Rabbit IgG (Novus Biologicals, NBP2-24891),
204 Rabbit IgG (ChromPure 011-000-003), Rat IgG (ChromPure, 012-000-003), Rat IgG (Biolegend,
205 400431), Rat IgG conjugated to Alexa Fluor 488 (Invitrogen, 53-4321-80). Slides were then
206 washed twice with PBS-T for 5 minutes and once with 1X PBS for 5 minutes. The following
207 secondary antibodies were used at a dilution of 1:200 for 1 hour at room temperature: Rat
208 conjugated to Alexa Fluor 488 (Invitrogen A11006), Rat conjugated to Alexa Fluor 568
209 (Invitrogen A11077), Rat conjugated to Alexa Fluor 647 (Invitrogen A-21247), Rabbit
210 conjugated to Alexa Fluor 568 (Invitrogen A11011), Rabbit conjugated to Alexa Fluor 647
211 (A27040). The following secondary antibodies were used at a dilution of 1:800 for 1 hour at
212 room temperature: Mouse conjugated to Alexa Fluor 647 (Invitrogen A21237), Streptavidin
213 conjugated to Alexa Fluor 568 (Invitrogen S11226), Streptavidin conjugated to Alexa Fluor 647
214 (Invitrogen S32357). DAPI (4',6-Diamidino-2-Phenylindole, Dilactate) (Biolegend, 422801) was
215 included during incubation with secondary antibodies at a concentration of 5 µg/ml. Slides were
216 then washed twice with PBS-T for 5 minutes and once with 1X PBS for 5 minutes. After
217 washing, slides were mounted using Prolong Gold Antifade Reagent with DAPI (Invitrogen

218 P36935). TUNEL staining was performed using the In Situ Cell Death Detection Kit TMR Red
219 (Roche, 12156792910) according to the manufacturer's instructions. Slides were imaged on a
220 Leica Fluorescent DMI 6000B wide-field microscope or a Nikon Ti Eclipse inverted microscope
221 with high-sensitivity confocal imaging at the Confocal and Specialized Microscopy Shared
222 Resource (CSMSR) Core at Columbia University. All images were analyzed in a blinded fashion
223 using FIJI software.

224 **2.6 Statistics**

225 Statistical analyses were conducted using GraphPad Prism v10.5. Data are presented as the mean
226 ± s.e.m., with all measurements obtained from distinct biological samples. All statistical tests
227 were performed using two-sided analyses. Normality was tested using the D'Agostino-Pearson
228 omnibus and, where appropriate, log transformation was applied to approximate normality.
229 Formal outliers were removed using a two-tailed Grubbs' test ($\alpha = 0.05$). Repeated measures data
230 were analyzed using two-way ANOVA with the Geisser-Greenhouse correction for sphericity and
231 Tukey's multiple comparisons test with individual variance estimation. For datasets involving
232 two independent variables, two-way ANOVA with Tukey's multiple comparisons test or Kruskal-
233 Wallis with Dunn's multiple comparisons test were used based on distribution. For datasets
234 involving five experimental groups, one-way ANOVA with Holm-Sidak's multiple comparisons
235 test or Kruskal-Wallis with Dunn's multiple comparisons test were used based on distribution.

236 Details of blood analysis can be found in the supplement.

237 **3. Results**

238 **3.1 Atherosclerosis Regression is Impaired with Moderate Cholesterol Lowering in *Jak2*^{VF}**
239 **CH**

240 To assess the effect of *Jak2*^{VF} CH on atherosclerosis regression, we placed *Jak2*^{VF} CH male mice
241 and controls on a western diet for 16 weeks and then induced cholesterol lowering using a
242 Helper-dependent Adenoviral vector containing the human LDL receptor gene (hDAD-hLDLR)
243 combined with a switch to chow diet for an additional 5 weeks (Figure 1A). Prior studies were
244 performed in female mice.[16,29] *Jak2*^{VF} CH male mice exhibited splenomegaly, lower body
245 weight, and increased RBCs, hematocrit, red blood cell distribution width (RDWc), and
246 neutrophils, mirroring previous findings in females (Supplemental Figure 1A-I).[29] In this model,
247 CD45.1+ cells are *Jak2*^{VF} in experimental mice and WT in controls. CD45.1+ neutrophils and
248 monocytes were elevated while CD45.1+ lymphocytes were reduced (Supplemental Figure 1J-
249 L). Plasma cholesterol was reduced in *Jak2*^{VF} CH mice on western diet (Figure 1B) similar to
250 previous findings in female mice and humans.[24,29,34] Plasma cholesterol remained moderately
251 elevated 10 days post-virus treatment but returned to pre-diet levels (~200-300 mg/dl) by the end
252 of the regression period (Figure 1B). At baseline, lesion area and necrotic core area were
253 significantly increased in the aortic root of male *Jak2*^{VF} CH mice compared to controls,
254 confirming that *Jak2*^{VF} CH worsens atherosclerosis in both male and female mice (Figure 1C-
255 E).[29] Moderate cholesterol lowering halted progression of lesion and necrotic core area in control
256 mice whereas *Jak2*^{VF} CH mice developed significantly larger necrotic cores and displayed a
257 strong trend toward increased lesion area (p=0.052) (Figure 1C-E). Consistent with previous
258 regression studies,[35,36] lesional collagen was increased in control mice after cholesterol lowering
259 with no significant change in *Jak2*^{VF} CH mice, further indicating impaired regression in the
260 *Jak2*^{VF} CH mice (Figure 1F,G). The most consistent phenotype found in atherosclerosis
261 regression studies has been a decrease in macrophage burden.[13,17-19,36] Macrophages were
262 significantly decreased in control mice but not in *Jak2*^{VF} CH mice after cholesterol lowering

263 (Figure 1H,I). These results indicate that atherosclerosis regression is impaired in *Jak2*^{VF} CH
264 with moderate cholesterol lowering.

265 We next assessed whether impaired regression in *Jak2*^{VF} CH mice was associated with persistent
266 inflammatory features in plaques. Necrotic, inflammatory cell death is mediated by activated
267 Gasdermin D (GasD) downstream of inflammasome activation.[37] We used an antibody to the
268 active N-terminal fragment of GasD to assess pyroptosis in plaques.[38] Total cleaved GasD in
269 plaques as well as cleaved GasD in the necrotic core were increased in *Jak2*^{VF} CH lesions at
270 baseline and were not reduced by cholesterol lowering (Figure 2A-C). However, macrophage-
271 specific cleaved GasD was decreased by cholesterol lowering in *Jak2*^{VF} CH lesions, suggesting
272 that macrophage pyroptosis had been suppressed by the time of harvest (Figure 2D,E).
273 Consistent with earlier findings in females, AIM2+ macrophages and phosphorylated histone
274 H2A.X (pγH2AX), an indicator of double stranded DNA break formation, were increased in
275 *Jak2*^{VF} CH lesions at baseline and were decreased by cholesterol lowering, suggesting reversal of
276 AIM2 inflammasome activation (Figure 2F-I).[29] Additionally, macrophage proliferation trended
277 higher at baseline in *Jak2*^{VF} CH mice and was significantly reduced by cholesterol lowering
278 (Figure 2J,K). Macrophage oxidized DNA was increased in control lesions and unchanged by
279 cholesterol lowering in *Jak2*^{VF} CH lesions (Figure 2L,M). These data suggest reversal of
280 macrophage AIM2 inflammasome activation and pyroptosis by moderate cholesterol lowering in
281 *Jak2*^{VF} CH mice, correlating with decreased macrophage proliferation and decreased DNA
282 damage response but not with oxidative DNA damage changes. The persistence of cleaved GasD
283 in the necrotic core area may reflect ongoing pyroptosis during the early phase of regression
284 when cholesterol levels were persistently elevated and could explain impaired regression in the
285 *Jak2*^{VF} mice.

286 **3.2 Cholesterol Lowering Restores Impaired Efferocytosis and increases TREM2+**
287 **Macrophages in *Jak2*^{VF} CH Lesions**

288 Atherosclerosis regression has been associated with improvements in pro-resolving features such
289 as increased macrophage efferocytosis, mer proto-oncogene tyrosine kinase (MerTK)
290 expression,[13,39,40] increased numbers of TREM2+ macrophages and limitation of necrotic core
291 formation in plaques.[16,41] During atherosclerosis progression, macrophage MerTK and TREM2
292 were suppressed in *Jak2*^{VF} CH mouse plaques as a result of interleukin-1 (IL-1) signaling from
293 mutant to wild-type (WT) cells.[38] Consistent with these studies, we found that macrophage
294 MerTK was decreased in *Jak2*^{VF} CH lesions at baseline compared to controls (Figure 3A,B).
295 MerTK levels were completely restored by cholesterol lowering (Figure 3A,B). Additionally, we
296 found that cholesterol lowering dramatically increased the percentage of macrophages positive
297 for TREM2 in both control and *Jak2*^{VF} CH lesions (Figure 3C,D). Consistent with these findings,
298 macrophage-associated TUNEL+ nuclei as a percentage of total lesional TUNEL+ nuclei, an
299 estimate of in situ efferocytosis,[14] were significantly decreased in *Jak2*^{VF} CH lesions at baseline
300 and restored by cholesterol lowering, (Figure 3E,F). Together, these data suggest that cholesterol
301 lowering restores impaired efferocytosis in *Jak2*^{VF} CH lesions and increases the proportion of
302 inflammation-resolving macrophages in lesions. Thus, macrophage inflammasome activation and
303 associated defects in efferocytosis were reversed by cholesterol lowering in *Jak2*^{VF} CH mice. The
304 increased necrotic core and decreased collagen content in these mice could reflect limited
305 resolution of hypercholesterolemia during the earlier phases of regression.

306 **3.3 More Effective Cholesterol Lowering Restores Atherosclerosis Regression**

307 To test this hypothesis, we performed a similar regression study but with more effective LDL
308 cholesterol lowering. Murine LDL does not bind as strongly to the human LDLR (employed in

309 Figure 1) as to the mouse LDLR.[42,43] Therefore, we employed an Adeno-Associated Virus
310 serotype 8 vector (AAV8) containing the mouse *Ldlr* gene which more effectively and more
311 quickly lowered cholesterol levels (Figure 4A). In this model, CD45.1+ cells are *Jak2*^{VF} in
312 experimental mice and WT in controls. Again, *Jak2*^{VF} CH mice exhibited splenomegaly, lower
313 body weight, and increased RBCs, hematocrit, and RDWc while CD45.1+ neutrophils and
314 monocytes were elevated, and these parameters were not appreciably changed by cholesterol
315 lowering (Supplemental Figure 2, Figure 4B). Consistent with the first study, lesion area and
316 necrotic core area were significantly increased in *Jak2*^{VF} CH mice at baseline. However, in
317 contrast to the first study, while both groups showed similar upwards trends, there was no
318 significant change in lesion area or necrotic core area in either group after aggressive LDL
319 lowering (Figure 4C-E). Furthermore, aggressive cholesterol lowering significantly increased
320 lesional collagen and decreased macrophage burden in both groups (Figure 4F-I). Analysis of
321 cleaved GasD showed an increase in macrophages in *Jak2*^{VF} mice at baseline that was reversed
322 by cholesterol lowering, and in contrast to the first study a decrease in cleaved GasD in the
323 necrotic core that appeared to involve both control and *Jak2*^{VF} CH mice (Supplemental Figure
324 3A-D). Consistent with the first study, double stranded DNA breaks (pγH2AX) were increased in
325 Jak2VF CH lesions at baseline and more strongly decreased by aggressive cholesterol lowering
326 along with a significant decrease in macrophage proliferation (Supplemental Figure 3E-H).
327 Additionally, macrophage MerTK was increased by aggressive cholesterol lowering in a manner
328 consistent with the first study (Supplemental Figure 3I,J). These results indicate that more
329 effective cholesterol lowering completely reversed inflammatory features and induced similar
330 levels of atherosclerosis regression in control and *Jak2*^{VF} CH lesions.

331 **3.4 Cholesterol Lowering Suppresses Proliferation of *Jak2^{VF}* Macrophages and increases c-**
332 **Myc+TREM2+ Macrophages**

333 The first two studies indicated that effective cholesterol lowering could reverse impaired
334 regression and the underlying cellular defects that promote AIM2 inflammasome activation.
335 However, in these studies *Jak2^{VF}* was active during progression and lesion area was increased at
336 baseline, potentially influencing the results. To simulate the situation where the *Jak2^{VF}* mutation
337 was acquired later in life after atherosclerosis had already developed, we performed a third study
338 in which *Jak2^{VF}* was activated in HSCs at the start of regression by using a tamoxifen-inducible
339 Scl-driven cre recombinase along with a floxed ZsGreen reporter allele (*Jak2^{VF} Scl* CH) to assess
340 cell genotype specific changes (Figure 5A). In addition to the two cholesterol lowering groups
341 (regression groups) we also included control and *Jak2^{VF}* mice that remained on the western diet
342 (progression groups). As expected, plasma cholesterol remained elevated in the progression
343 groups but was markedly and rapidly decreased in both regression groups (Figure 5B). In this
344 model, cells double positive for CD45.1 and CD45.2 are *Jak2^{VF}* in experimental mice and WT in
345 controls. The *Jak2^{VF}* phenotype was partially apparent as indicated by increased spleen weights,
346 RDWc, and hematocrit as well as expansion of CD45.1+CD45.2+ blood monocytes and
347 neutrophils, but less pronounced than in the earlier studies when *Jak2^{VF}* was activated prior to
348 Western diet feeding (Supplemental Figure 4).

349 Compared to the earlier models, the impact of *Jak2^{VF}* on lesion progression was less pronounced
350 which likely reflects the shorter period of *Jak2^{VF}* activation (Supplemental Figure 5A-C).
351 However, consistent with the earlier studies, the necrotic core significantly worsened in the
352 *Jak2^{VF} Scl* CH progression mice but not in the control *Scl* mice compared to baseline, while the
353 necrotic core was not significantly changed in either regression group compared to baseline

354 (Supplemental Figure 5C). Additionally, macrophage burden was similarly decreased in both
355 regression groups, (Supplemental Figure 5D,E). These studies further support that aggressive
356 cholesterol lowering similarly promotes regression in control and *Jak2*^{VF} CH mice, compared to
357 progression or baseline groups, in mice with *Jak2*^{VF} only activated at the beginning of the
358 regression period.

359 Cleaved GasD was increased in *Jak2*^{VF} CH lesions compared to baseline and trended lower
360 (p=.06) after cholesterol lowering, consistent with aggressive cholesterol lowering reversing
361 pyroptosis in lesions (Figure 5C,D). In the *Jak2*^{VF} CH progression group, proliferation was
362 significantly increased in *Jak2*^{VF} (green) macrophages but not in WT (non-green) macrophages
363 indicating a mutant cell specific effect, as seen previously.[29] Notably, this was reversed by
364 cholesterol lowering indicating that proliferation of the *Jak2*^{VF} cells was highly dependent on
365 LDL cholesterol levels (Figure 5E-G). Consistently, the DNA damage response (pγH2AX) was
366 significantly increased in *Jak2*^{VF} cells, and this was reversed by cholesterol lowering while WT
367 cells showed no significant changes within *Jak2*^{VF} CH lesions (Figure 5H-J). This suggests that
368 cell autonomous proliferation and associated formation of double stranded DNA breaks is
369 reversed by cholesterol lowering in lesions of *Jak2*^{VF} CH mice.

370 Given that a proliferative efferocytic population with high c-Myc expression has been described
371 during regression,[13,39] we assessed c-Myc expression along with TREM2. In contrast to the
372 decreases in Ki67, macrophage c-Myc and c-Myc+TREM2^{Hi} macrophages were increased
373 during regression in both control and *Jak2*^{VF} mice, suggesting a selective increase of TREM2+,
374 anti-inflammatory macrophages despite a decrease in total macrophages (Figure 6).

375 **4. Discussion**

376 We previously showed that the combination of LDL lowering and *Jak2*^{VF} genetic inactivation
377 induced fibrous cap thickening and increased TREM2^{Hi} macrophages in *Jak2*^{VF} CH mice.[16]
378 Given the propensity of plaque *Jak2*^{VF} mutant cells to proliferation, DNA damage, and AIM2
379 inflammasome activation,[29] we hypothesized that LDL lowering alone would be insufficient to
380 induce plaque regression in *Jak2*^{VF} mice. While this proved to be the case with moderate LDL
381 lowering, aggressive cholesterol lowering produced plaque regression (or halted progression)
382 similarly in controls and *Jak2*^{VF} CH mice. Surprisingly, LDL lowering reversed the major
383 cellular changes in *Jak2*^{VF} macrophages that have been associated with athero-progression. This
384 included reduced AIM2 expression and pyroptosis and increased MerTK, TREM2 and in situ
385 efferocytosis that have all been mechanistically linked in prior studies of *Jak2*^{VF} mice.[38] Whereas
386 we previously considered glycolytic mitochondrial ROS production and oxidative DNA damage
387 as a likely mechanism underlying AIM2 inflammasome activation, the reversal of pyroptosis by
388 cholesterol lowering was not associated with reduced oxidized DNA. Rather, decreased
389 macrophage proliferation and reduced replication stress appears to be the major mechanism
390 underlying reversal of pyroptosis.

391 Studies of atherosclerosis regression induced by LDL lowering in mouse models have revealed
392 multiple underlying mechanisms[44] including macrophage emigration,[45] decreased monocyte
393 entry[46] and a key role of acquired immunity and T-regs.[17] Similar to macrophage proliferation
394 being a major factor accounting for increased macrophage number during advanced
395 atherosclerosis progression,[47] suppression of proliferation is the predominant mechanism
396 decreasing macrophage burden during regression.[35] Our studies suggest that decreased
397 proliferation of *Jak2*^{VF} macrophages is also a key mechanism decreasing macrophage burden
398 during atherosclerosis regression. Moreover, decreased proliferation was associated with reduced

399 DNA damage response, AIM2 expression and pyroptosis in *Jak2*^{VF} CH lesions, suggesting
400 decreased replication induced DNA damage as the key underlying mechanism responding to
401 cholesterol lowering.

402 Paradoxically, despite the overall reduction in macrophage burden, during regression there may
403 also be a relative increase in a proliferative set of efferocytotic macrophages that also express c-
404 myc expression and contribute to plaque stability.[13,14] However, in addition to a potential role in
405 cell proliferation c-myc has an additional role in Akt signaling and cell survival.[48,49] Previously,
406 we observed a 4-fold increase in TREM2^{Hi} macrophages during atherosclerosis regression
407 induced by both LDL lowering and *Jak2*^{VF} inactivation in *Jak2*^{VF} CH mice.[16] In the present
408 study, we found that LDL lowering alone led to a marked increase in TREM2 staining in
409 macrophages, as well as elevated c-myc expression specifically within TREM2^{Hi} macrophages,
410 in both control and mutant mice. This contrasts with the decreased proliferation and DNA
411 damage response found specifically in the *Jak2*^{VF} macrophages. Our findings together suggest
412 that during regression there is an increase in TREM2^{Hi}, c-myc and MerTK expressing
413 macrophages either through increased proliferation or increased survival of these subsets that
414 then have beneficial effects on efferocytosis and plaque stability. Given that inflammasome
415 activation and IL-1 release have been linked to reduced MerTK and TREM2 as a result of A
416 Disintegrin And Metalloproteinase 17 (ADAM17)-mediated cleavage,[39,50] the increase in this
417 pro-resolving macrophage population may in part be secondary to reduced cholesterol-induced
418 inflammasome activation. Although IL-1β antibodies have been shown to inhibit atherosclerosis
419 regression in *Apoe*$^{-/-}$ mice,[15] IL-1β antibodies improved lesion stability in hypercholesterolemic
420 *Jak2*^{VF} CH mice.[16,29] Elevated IL-1β signaling as a result of increased pyroptosis in *Jak2*^{VF} CH
421 lesions is decreased in the present study as a result of LDL lowering. Combined, these results

422 suggest that excessive IL-1β activation is pro-atherogenic in the context of hypercholesterolemia
423 while a basal level of IL-1β activation may be required for lesion resolution after cholesterol
424 lowering which is blocked when IL-1β antibodies are present.

425 The history of LDL lowering guidelines has been to recommend progressively lower targets
426 based on clinical trial evidence. Current recommendations suggest an LDL cholesterol target
427 below 70 mg/dl for patients with established ACVD or in certain high-risk groups.[51] Statin use
428 has been associated with improved outcomes in human myeloproliferative neoplasm (MPN)
429 patients and was associated with a 37% reduction in the risk of thrombosis in patients who had
430 polycythemia vera or essential thrombocythemia as well as a 22% reduction in all-cause
431 mortality.[52] While data from mice should be extrapolated to humans with caution, the AIM2
432 inflammasome seems to increase ACVD risk in both mice and humans carrying the *Jak2*^{VF}
433 mutation.[30] The present preclinical study adds mechanistic findings to support the idea that
434 aggressive LDL-C lowering in *Jak2*^{VF} MPN patients would reduce ACVD risk.

Acknowledgements

The authors thank Wenli Liu for assistance and support during the course of this study. This study used the Confocal and Specialized Microscopy Shared Resource of the Herbert Irving Comprehensive Cancer Center at Columbia University, funded in part through NIH/NCI Cancer Center Support Grant P30CA013696. Additionally, this study used the resources of the Herbert Irving Comprehensive Cancer Center Flow Cytometry Shared Resources funded in part through Center Grant P30CA013696.

Sources of Funding

This work was supported by grants from the National Institutes of Health and The National Heart, Lung, and Blood Institute: HL155431, HL107653HL170157-02, P01HL172741 to A.R.T and HL148071 to N.W.

Disclosures

A.R.T. is a consultant for CSL Behring and is on the scientific advisory board of Beren Therapeutics. The remaining authors declare no competing financial interests.

Author Contribution Statement

B.H., A.T., N.W., T.F. made substantial contributions to conception, design, data acquisition, analysis, and interpretation. They also drafted and critically reviewed the manuscript for intellectual content. M.T., K.A., C.H., S.S., and T.X. contributed to data acquisition and analysis.

Data Availability Statement

The datasets generated for this study are available from the corresponding author upon reasonable request.

References

1. Martin SS, Aday AW, Almarzooq ZI, Anderson CAM, Arora P, Avery CL, Baker-Smith CM, Barone Gibbs B, Beaton AZ, Boehme AK, Commodore-Mensah Y, Currie ME, Elkind MSV, Evenson KR, Generoso G, Heard DG, Hiremath S, Johansen MC, Kalani R, Kazi DS, Ko D, Liu J, Magnani JW, Michos ED, Mussolino ME, Navaneethan SD, Parikh NI, Perman SM, Poudel R, Rezk-Hanna M, Roth GA, Shah NS, St-Onge MP, Thacker EL, Tsao CW, Urbut SM, Van Spall HGC, Voeks JH, Wang NY, Wong ND, Wong SS, Yaffe K, Palaniappan LP; American Heart Association Council on Epidemiology and Prevention Statistics Committee and Stroke Statistics Subcommittee. 2024 Heart Disease and Stroke Statistics: A Report of US and Global Data From the American Heart Association. *Circulation* 2024;**149**:e347–e913.
2. Vallejo-Vaz AJ, Fayyad R, Boekholdt SM, Hovingh GK, Kastelein JJP, Melamed S, Barter P, Waters DD, Ray KK. Triglyceride-rich lipoprotein cholesterol and risk of cardiovascular events among patients receiving statin therapy in the TNT trial. *Circulation* 2018;**138**:770–781.
3. Cannon CP, Blazing MA, Giugliano RP, McCagg A, White JA, Theroux P, Darius H, Lewis BS, Ophuis TO, Jukema JW, De Ferrari GM, Ruzyllo W, De Lucca P, Im K, Bohula EA, Reist C, Wiviott SD, Tershakovec AM, Musliner TA, Braunwald E, Califf RM; IMPROVE-IT Investigators. Ezetimibe added to statin therapy after acute coronary syndromes. *N Engl J Med* 2015;**372**:2387–2397.
4. Sabatine MS, Giugliano RP, Keech AC, Honarpour N, Wiviott SD, Murphy SA, Kuder JF, Wang H, Liu T, Wasserman SM, Sever PS, Pedersen TR; FOURIER Steering

478 Committee and Investigators. Evolocumab and clinical outcomes in patients with
479 cardiovascular disease. *N Engl J Med* 2017;**376**:1713–1722.
480 5. Nidorf SM, Fiolet ATL, Mosterd A, Eikelboom JW, Schut A, Opstal TSJ, The SHK, Xu
481 XF, Ireland MA, Lenderink T, Latchem D, Hoogslag P, Jerzewski A, Nierop P, Whelan A,
482 Hendriks R, Swart H, Schaap J, Kuijper AFM, van Hessen MWJ, Saklani P, Tan I,
483 Thompson AG, Morton A, Judkins C, Bax WA, Dirksen M, Alings M, Hankey GJ,
484 Budgeon CA, Tijssen JGP, Cornel JH, Thompson PL; LoDoCo2 Trial Investigators.
485 Colchicine in patients with chronic coronary disease. *N Engl J Med* 2020;**383**:1838–
486 1847.
487 6. U.S. Food and Drug Administration. Drug approval package: Lodoco (colchicine) tablets,
488 0.5 mg. Approval letter. Published June 16, 2023. Accessed July 5, 2025.
489 https://www.accessdata.fda.gov/drugsatfda_docs/nda/2024/215727Orig1s000Approv.pdf
490 7. Ridker PM, Everett BM, Thuren T, MacFadyen JG, Chang WH, Ballantyne CM, Fonseca
491 F, Nicolau J, Koenig W, Anker SD, Kastelein JJP, Cornel JH, Pais P, Pella D, Genest J,
492 Cifkova R, Lorenzatti A, Forster T, Kobalava Z, Vida-Simiti L, Flather M, Shimokawa H,
493 Ogawa H, Dellborg M, Rossi PRF, Troquay RPT, Libby P, Glynn RJ; CANTOS Trial
494 Group. Antiinflammatory therapy with canakinumab for atherosclerotic disease. *N Engl J*
495 *Med* 2017;**377**:1119–1131.
496 8. Ridker PM. From C-reactive protein to interleukin-6 to interleukin-1: moving upstream to
497 identify novel targets for atheroprotection. *Circ Res* 2016;**118**:145–156.
498 9. Yalcinkaya M, Liu W, Xiao T, Abramowicz S, Wang R, Wang N, Westerterp M, Tall AR.
499 Cholesterol trafficking to the ER leads to the activation of CaMKII/JNK/NLRP3 and
500 promotes atherosclerosis. *J Lipid Res* 2024;**65**:100534.

501 10. Westerterp M, Fotakis P, Ouimet M, Bochem AE, Zhang H, Molusky MM, Wang W,
502 Abramowicz S, la Bastide-van Gemert S, Wang N, Welch CL, Reilly MP, Stroes ES,
503 Moore KJ, Tall AR. Cholesterol efflux pathways suppress inflammasome activation,
504 NETosis, and atherogenesis. *Circulation* 2018;**138**:898–912.
505 11. Yalcinkaya M, Fotakis P, Liu W, Endo-Umeda K, Dou H, Abramowicz S, Xiao T, Libby
506 P, Wang N, Tall AR, Westerterp M. Cholesterol accumulation in macrophages drives
507 NETosis in atherosclerotic plaques via IL-1β secretion. *Cardiovasc Res* 2023;**119**:969–
508 981.
509 12. Sheedy FJ, Grebe A, Rayner KJ, Kalantari P, Ramkhelawon B, Carpenter SB, Becker CE,
510 Ediriweera HN, Mullick AE, Golenbock DT, Stuart LM, Latz E, Fitzgerald KA, Moore
511 KJ. CD36 coordinates NLRP3 inflammasome activation by facilitating intracellular
512 nucleation of soluble ligands into particulate ligands in sterile inflammation. *Nat*
513 *Immunol* 2013;**14**:812–820.
514 13. Gerlach BD, Ampomah PB, Yurdagul A Jr, Liu C, Lauring MC, Wang X, Kasikara C,
515 Kong N, Shi J, Tao W, Tabas I. Efferocytosis induces macrophage proliferation to help
516 resolve tissue injury. *Cell Metab* 2021;**33**:2445–2463.e8.
517 14. Yurdagul A Jr, Subramanian M, Wang X, Crown SB, Ilkayeva OR, Darville L, Kolluru
518 GK, Rymond CC, Gerlach BD, Zheng Z, Kuriakose G, Kevil CG, Koomen JM,
519 Cleveland JL, Muoio DM, Tabas I. Macrophage metabolism of apoptotic cell-derived
520 arginine promotes continual efferocytosis and resolution of injury. *Cell Metab*
521 2020;**31**:518–533.e10.
522 15. Karnewar S, Karnewar V, Deaton RA, Shankman LS, Benavente ED, Williams CM,
523 Bradley X, Alencar GF, Bulut GB, Kirmani S, Baylis RA, Zunder ER, den Ruijter HM,

524 Pasterkamp G, Owens GK. IL-1β inhibition partially negates the beneficial effects of
525 diet-induced atherosclerosis regression in mice. *Arterioscler Thromb Vasc Biol*
526 2024;**44**:1379–1392.
527 16. Fidler TP, Dunbar A, Kim E, Hardaway B, Pauli J, Xue C, Abramowicz S, Xiao T,
528 O'Connor K, Sachs N, Wang N, Maegdefessel L, Levine R, Reilly MP, Tall AR.
529 Suppression of IL-1β promotes beneficial accumulation of fibroblast-like cells in
530 atherosclerotic plaques in clonal hematopoiesis. *Nat Cardiovasc Res* 2024;**3**:60–75.
531 17. Sharma M, Schlegel MP, Afonso MS, Brown EJ, Rahman K, Weinstock A, Sansbury BE,
532 Corr EM, van Solingen C, Koelwyn GJ, Shanley LC, Beckett L, Peled D, Lafaille JJ,
533 Spite M, Loke P, Fisher EA, Moore KJ. Regulatory T cells license macrophage pro-
534 resolving functions during atherosclerosis regression. *Circ Res* 2020;**127**:335–353.
535 18. Zhang X, Rotllan N, Canfrán-Duque A, Sun J, Toczek J, Moshnikova A, Malik S, Price
536 NL, Araldi E, Zhong W, Sadeghi MM, Andreev OA, Bahal R, Reshetnyak YK, Suárez Y,
537 Fernández-Hernando C. Targeted suppression of miRNA-33 using pHLIP improves
538 atherosclerosis regression. *Circ Res* 2022;**131**:77–90.
539 19. Basu D, Hu Y, Huggins LA, Mullick AE, Graham MJ, Wietecha T, Barnhart S, Mogul A,
540 Pfeiffer K, Zirlik A, Fisher EA, Bornfeldt KE, Willecke F, Goldberg IJ. Novel reversible
541 model of atherosclerosis and regression using oligonucleotide regulation of the LDL
542 receptor. *Circ Res* 2018;**122**:560–567.
543 20. Tall AR, Fuster JJ. Clonal hematopoiesis in cardiovascular disease and therapeutic
544 implications. *Nat Cardiovasc Res* 2022;**1**:116–124.
545 21. Jaiswal S, Fontanillas P, Flannick J, Manning A, Grauman PV, Mar BG, Lindsley RC,
546 Mermel CH, Burtt N, Chavez A, Higgins JM, Moltchanov V, Kuo FC, Kluk MJ,

547 Henderson B, Kinnunen L, Koistinen HA, Ladenvall C, Getz G, Correa A, Banahan BF,
548 Gabriel S, Kathiresan S, Stringham HM, McCarthy MI, Boehnke M, Tuomilehto J,
549 Haiman CA, Groop L, Atzmon G, Wilson JG, Neuberg D, Altshuler D, Ebert BL. Age-
550 related clonal hematopoiesis associated with adverse outcomes. *N Engl J Med*
551 2014;**371**:2488–2498.
552 22. Jaiswal S, Natarajan P, Silver AJ, Gibson CJ, Bick AG, Shvartz E, McConkey M, Gupta
553 N, Gabriel S, Ardissino D, Baber U, Mehran R, Fuster V, Danesh J, Frossard P, Saleheen
554 D, Melander O, Sukhova GK, Neuberg D, Libby P, Kathiresan S, Ebert BL. Clonal
555 hematopoiesis and risk of atherosclerotic cardiovascular disease. *N Engl J Med*
556 2017;**377**:111–121.
557 23. Kar SP, Quiros PM, Gu M, Jiang T, Mitchell J, Langdon R, Iyer V, Barcena C,
558 Vijayabaskar MS, Fabre MA, Carter P, Petrovski S, Burgess S, Vassiliou GS. Genome-
559 wide analyses of 200 453 individuals yield new insights into the causes and consequences
560 of clonal hematopoiesis. *Nat Genet* 2022;**54**:1155–1166.
561 24. Bick AG, Weinstock JS, Nandakumar SK, Fulco CP, Bao EL, Zekavat SM, Szeto MD,
562 Liao X, Leventhal MJ, Nasser J, Chang K, Laurie C, Burugula BB, Gibson CJ, Lin AE,
563 Taub MA, Aguet F, Ardlie K, Mitchell BD, Barnes KC, Moscati A, Fornage M, Redline
564 S, Psaty BM, Silverman EK, Weiss ST, Palmer ND, Vasan RS, Burchard EG, Kardia
565 SLR, He J, Kaplan RC, Smith NL, Arnett DK, Schwartz DA, Correa A, de Andrade M,
566 Guo X, Konkle BA, Custer B, Peralta JM, Gui H, Meyers DA, McGarvey ST, Chen IY,
567 Shoemaker MB, Peyser PA, Broome JG, Gogarten SM, Wang FF, Wong Q, Montasser
568 ME, Daya M, Kenny EE, North KE, Launer LJ, Cade BE, Bis JC, Cho MH, Lasky-Su J,
569 Bowden DW, Cupples LA, Mak ACY, Becker LC, Smith JA, Kelly TN, Aslibekyan S,

570 Heckbert SR, Tiwari HK, Yang IV, Heit JA, Lubitz SA, Johnsen JM, Curran JE, Wenzel
571 SE, Weeks DE, Rao DC, Darbar D, Moon JY, Tracy RP, Buth EJ, Rafaels N, Loos RJF,
572 Durda P, Liu Y, Hou L, Lee J, Kachroo P, Freedman BI, Levy D, Bielak LF, Hixson JE,
573 Floyd JS, Whitsel EA, Ellinor PT, Irvin MR, Fingerlin TE, Raffield LM, Armasu SM,
574 Wheeler MM, Sabino EC, Blangero J, Williams LK, Levy BD, Sheu WH, Roden DM,
575 Boerwinkle E, Manson JE, Mathias RA, Desai P, Taylor KD, Johnson AD; NHLBI Trans-
576 Omics for Precision Medicine Consortium; Auer PL, Kooperberg C, Laurie CC,
577 Blackwell TW, Smith AV, Zhao H, Lange E, Lange L, Rich SS, Rotter JI, Wilson JG,
578 Scheet P, Kitzman JO, Lander ES, Engreitz JM, Ebert BL, Reiner AP, Jaiswal S, Abecasis
579 G, Sankaran VG, Kathiresan S, Natarajan P. Inherited causes of clonal haematopoiesis in
580 97,691 whole genomes. *Nature* 2020;**586**:763–768.
581 25. Cordua S, Kjaer L, Skov V, Pallisgaard N, Hasselbalch HC, Ellervik C. Prevalence and
582 phenotypes of JAK2 V617F and calreticulin mutations in a Danish general population.
583 *Blood* 2019;**134**:469–479.
584 26. Wang S, Luo X, Hu S, Zhao C, Sun Q, Zeng M, Bao X, Wang Y, Wu F, Yang Y, Lv Y, Bai
585 X, Hao W, Liu M, Yi B, Chen Y, Meng W, Li J, Li M, Huang J, Wu T, Zhao Y, Zhang Z,
586 An J, Libby P, Jia H, Yu B. Plaque erosion risk and JAK2 V617F variant. *Eur Heart J*
587 2025;**46**:2205–2219.
588 27. Molinaro R, Sellar RS, Vromman A, Sausen G, Folco E, Sukhova GK, McConke ME,
589 Corbo C, Ebert BL, Libby P. The clonal hematopoiesis mutation Jak2V617F aggravates
590 endothelial injury and thrombosis in arteries with erosion-like intimas. *Int J Cardiol*
591 2024;**409**:132184.

592 28. Liu W, Pircher J, Schuermans A, Ul Ain Q, Zhang Z, Honigberg MC, Yalcinkaya M,
593 Nakao T, Pournamadri A, Xiao T, Hajebrahimi MA, Wasner L, Stegner D, Petzold T,
594 Natarajan P, Massberg S, Tall AR, Schulz C, Wang N. Jak2 V617F clonal hematopoiesis
595 promotes arterial thrombosis via platelet activation and cross talk. *Blood* 2024;**143**:1539–
596 1550.
597 29. Fidler TP, Xue C, Yalcinkaya M, Hardaway B, Abramowicz S, Xiao T, Liu W, Thomas
598 DG, Hajebrahimi MA, Pircher J, Silvestre-Roig C, Kotini AG, Luchsinger LL, Wei Y,
599 Westerterp M, Snoeck HW, Papapetrou EP, Schulz C, Massberg S, Soehnlein O, Ebert
600 BL, Levine RL, Reilly MP, Libby P, Wang N, Tall AR. The AIM2 inflammasome
601 exacerbates atherosclerosis in clonal haematopoiesis. *Nature* 2021;**592**:296–301.
602 30. Yu Z, Fidler TP, Ruan Y, Vlasschaert C, Nakao T, Uddin MM, Mack T, Niroula A,
603 Heimlich JB, Zekavat SM, Gibson CJ, Griffin GK, Wang Y, Peloso GM, Heard-Costa N,
604 Levy D, Vasan RS, Aguet F, Ardlie KG, Taylor KD, Rich SS, Rotter JI, Libby P, Jaiswal
605 S, Ebert BL, Bick AG, Tall AR, Natarajan P. Genetic modification of inflammation- and
606 clonal hematopoiesis-associated cardiovascular risk. *J Clin Invest* 2023;**133**:e168597.
607 31. Rathinam VA, Fitzgerald KA. Inflammasome complexes: emerging mechanisms and
608 effector functions. *Cell* 2016;**165**:792–800.
609 32. Mullally A, Lane SW, Ball B, Megerdichian C, Okabe R, Al-Shahrour F, Paktinat M,
610 Haydu JE, Housman E, Lord AM, Wernig G, Kharas MG, Mercher T, Kutok JL, Gilliland
611 DG, Ebert BL. Physiological Jak2V617F expression causes a lethal myeloproliferative
612 neoplasm with differential effects on hematopoietic stem and progenitor cells. *Cancer*
613 *Cell* 2010;**17**:584–596.

614 33. Pan H, Xue C, Auerbach BJ, Fan J, Bashore AC, Cui J, Yang DY, Trignano SB, Liu W,
615 Shi J, Ihuegbu CO, Bush EC, Worley J, Vlahos L, Laise P, Solomon RA, Connolly ES,
616 Califano A, Sims PA, Zhang H, Li M, Reilly MP. Single-cell genomics reveals a novel
617 cell state during smooth muscle cell phenotypic switching and potential therapeutic
618 targets for atherosclerosis in mouse and human. *Circulation* 2020;**142**:2060–2075.
619 34. Kar SP, Quiros PM, Gu M, Jiang T, Mitchell J, Langdon R, Iyer V, Barcena C,
620 Vijayabaskar MS, Fabre MA, Carter P, Petrovski S, Burgess S, Vassiliou GS. Genome-
621 wide analyses of 200 453 individuals yield new insights into the causes and consequences
622 of clonal hematopoiesis. *Nat Genet* 2022;**54**:1155–1166.
623 35. Härdtner C, Kornemann J, Krebs K, Ehlert CA, Jander A, Zou J, Starz C, Rauterberg S,
624 Sharipova D, Dufner B, Hoppe N, Dederichs TS, Willecke F, Stachon P, Heidt T, Wolf D,
625 von Zur Mühlen C, Madl J, Kohl P, Kaeser R, Boettler T, Pieterman EJ, Princen HMG,
626 Ho-Tin-Noé B, Swirski FK, Robbins CS, Bode C, Zirlik A, Hilgendorf I. Inhibition of
627 macrophage proliferation dominates plaque regression in response to cholesterol
628 lowering. *Basic Res Cardiol* 2020;**115**:78.
629 36. Peled M, Nishi H, Weinstock A, Barrett TJ, Zhou F, Quezada A, Fisher EA. A wild-type
630 mouse-based model for the regression of inflammation in atherosclerosis. *PLoS One*
631 2017;**12**:e0173975.
632 37. Broz P. Pyroptosis: molecular mechanisms and roles in disease. *Cell Res* 2025;**35**:334–
633 344.
634 38. Liu W, Hardaway BD, Kim E, Pauli J, Wettich JL, Yalcinkaya M, Hsu CC, Xiao T, Reilly
635 MP, Tabas I, Maegdefessel L, Schlepckow K, Haass C, Wang N, Tall AR. Inflammatory

636 crosstalk impairs phagocytic receptors and aggravates atherosclerosis in clonal
637 hematopoiesis in mice. *J Clin Invest* 2024;**135**:e182939.
638 39. Ngai D, Schilperoort M, Tabas I. Efferocytosis-induced lactate enables the proliferation
639 of pro-resolving macrophages to mediate tissue repair. *Nat Metab* 2023;**5**:2206–2219.
640 40. Sukka SR, Ampomah PB, Darville LNF, Ngai D, Wang X, Kuriakose G, Xiao Y, Shi J,
641 Koomen JM, McCusker RH, Tabas I. Efferocytosis drives a tryptophan metabolism
642 pathway in macrophages to promote tissue resolution. *Nat Metab* 2024;**6**:1736–1755.
643 41. Patterson MT, Xu Y, Hillman H, Osinski V, Schrank PR, Kennedy AE, Barrow F, Zhu A,
644 Tollison S, Shekhar S, Stromnes IM, Tassi I, Wu D, Revelo XS, Binstadt BA, Williams
645 JW. Trem2 agonist reprograms foamy macrophages to promote atherosclerotic plaque
646 stability — brief report. *Arterioscler Thromb Vasc Biol* 2024;**44**:1646–1657.
647 42. Corsini A, Mazzotti M, Villa A, Maggi FM, Bernini F, Romano L, Romano C, Fumagalli
648 R, Catapano AL. Ability of the LDL receptor from several animal species to recognize
649 the human apo B binding domain: studies with LDL from familial defective apo B-100.
650 *Atherosclerosis* 1992;**93**:95–103.
651 43. Innerarity TL, Pitas RE, Mahley RW. Disparities in the interaction of rat and human
652 lipoproteins with cultured rat fibroblasts and smooth muscle cells: requirements for
653 homology for receptor binding activity. *J Biol Chem* 1980;**255**:11163–11172.
654 44. Lin JD, Nishi H, Poles J, Niu X, McCauley C, Rahman K, Brown EJ, Yeung ST, Vozhilla
655 N, Weinstock A, Ramsey SA, Fisher EA, Loke P. Single-cell analysis of fate-mapped
656 macrophages reveals heterogeneity, including stem-like properties, during atherosclerosis
657 progression and regression. *JCI Insight* 2019;**4**:e124574.

658 45. Feig JE, Pineda-Torra I, Sanson M, Bradley MN, Vengrenyuk Y, Bogunovic D, Gautier
659 EL, Rubinstein D, Hong C, Liu J, Wu C, van Rooijen N, Bhardwaj N, Garabedian M,
660 Tontonoz P, Fisher EA. LXR promotes the maximal egress of monocyte-derived cells
661 from mouse aortic plaques during atherosclerosis regression. *J Clin Invest*
662 2010;**120**:4415–4424.
663 46. Nagareddy PR, Murphy AJ, Stirzaker RA, Hu Y, Yu S, Miller RG, Ramkhelawon B,
664 Distel E, Westerterp M, Huang LS, Schmidt AM, Orchard TJ, Fisher EA, Tall AR,
665 Goldberg IJ. Hyperglycaemia promotes myelopoiesis and impairs the resolution of
666 atherosclerosis. *Cell Metab* 2013;**17**:695–708.
667 47. Robbins CS, Hilgendorf I, Weber GF, Theurl I, Iwamoto Y, Figueiredo JL, Gorbatov R,
668 Sukhova GK, Gerhardt LM, Smyth D, Zavitz CC, Shikatani EA, Parsons M, van Rooijen
669 N, Lin HY, Husain M, Libby P, Nahrendorf M, Weissleder R, Swirski FK. Local
670 proliferation dominates lesional macrophage accumulation in atherosclerosis. *Nat Med*
671 2013;**19**:1166–1172.
672 48. Miller DM, Thomas SD, Islam A, Muench D, Sedoris K. c-Myc and cancer metabolism.
673 *Clin Cancer Res* 2012;**18**:5546–5553.
674 49. Wise DR, DeBerardinis RJ, Mancuso A, Sayed N, Zhang XY, Pfeiffer HK, Nissim I,
675 Daikhin E, Yudkoff M, McMahon SB, Thompson CB. Myc regulates a transcriptional
676 program that stimulates mitochondrial glutaminolysis and leads to glutamine addiction.
677 *Proc Natl Acad Sci U S A* 2008;**105**:18782–18787.
678 50. Endo-Umeda K, Kim E, Thomas DG, Liu W, Dou H, Yalcinkaya M, Abramowicz S, Xiao
679 T, Antonson P, Gustafsson JÅ, Makishima M, Reilly MP, Wang N, Tall AR. Myeloid
680 LXR (liver X receptor) deficiency induces inflammatory gene expression in foamy

681 macrophages and accelerates atherosclerosis. *Arterioscler Thromb Vasc Biol*
682 2022;**42**:719–731.
683 51. Virani SS, Newby LK, Arnold SV, Bittner V, Brewer LC, Demeter SH, Dixon DL, Fearon
684 WF, Hess B, Johnson HM, Kazi DS, Kolte D, Kumbhani DJ, LoFaso J, Mahtta D, Mark
685 DB, Minissian M, Navar AM, Patel AR, Piano MR, Rodriguez F, Talbot AW, Taqueti VR,
686 Thomas RJ, van Diepen S, Wiggins B, Williams MS; Peer Review Committee Members.
687 2023 AHA/ACC/ACCP/ASPC/NLA/PCNA guideline for the management of patients
688 with chronic coronary disease: a report of the American Heart Association/American
689 College of Cardiology Joint Committee on Clinical Practice Guidelines. *Circulation*
690 2023;**148**:e9–e119.
691 52. Podoltsev NA, Wang R, Shallis RM, Stempel JM, Di M, Neparidze N, Zeidan AM,
692 Huntington SF, Giri S, Hull SC, Gore SD, Ma X. Statin use, survival and incidence of
693 thrombosis among older patients with polycythemia vera and essential thrombocythemia.
694 *Cancer Med* 2023;**12**:18889–18900.

695

Figure 1

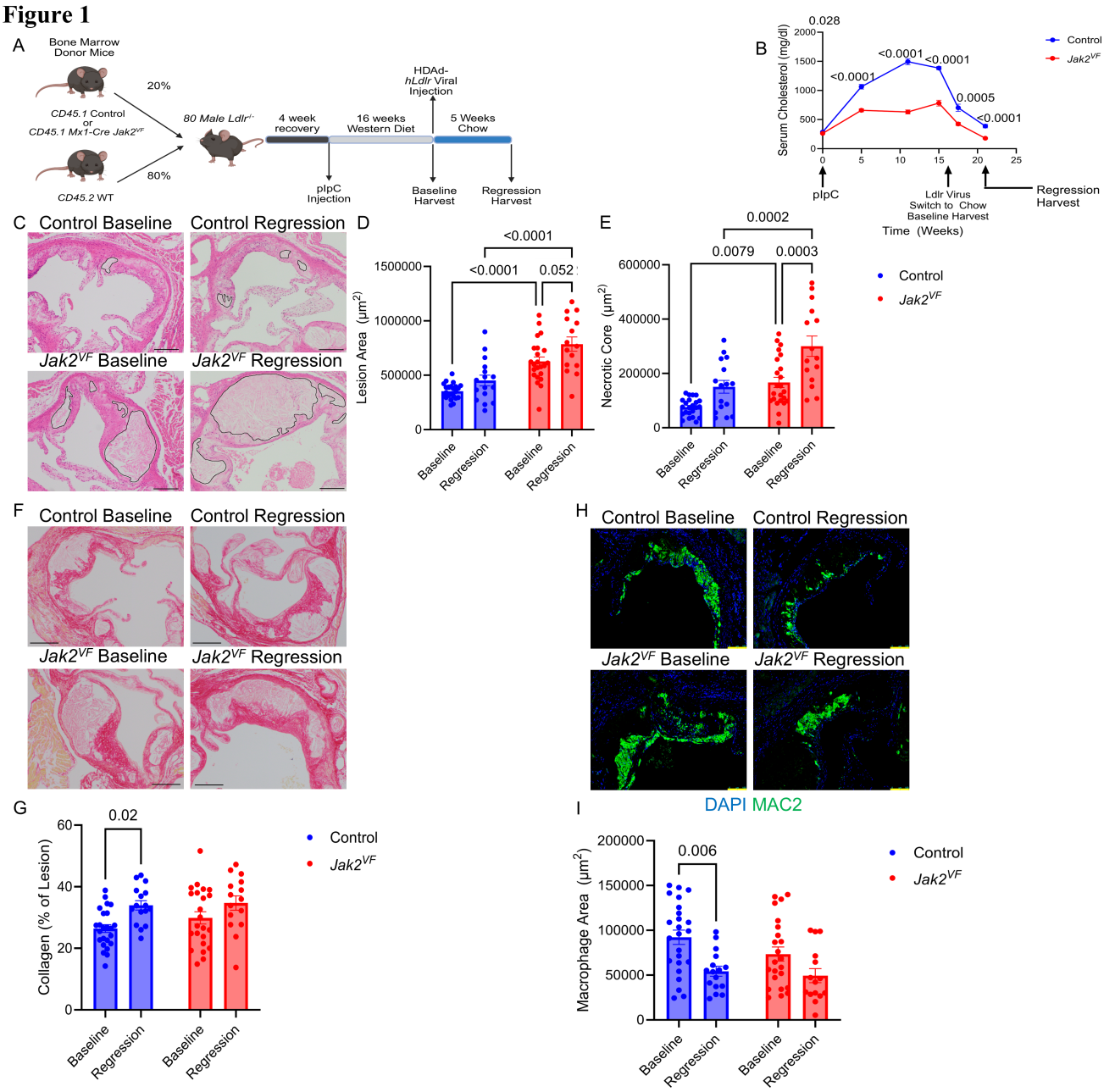
A
Bone Marrow Donor Mice
CD45.1 Control or CD45.1 Mx1-Cre Jak2VF
CD45.2 WT
20%
80%
80 Male Ldlr-/-
4 week recovery
16 weeks Western Diet
HDAd-hLdlr Viral Injection
5 Weeks Chow
pIpC Injection
Baseline Harvest
Regression Harvest
B
Serum Cholesterol (mg/dl)
Time (Weeks)
Control
Jak2VF
pIpC
Ldlr Virus Switch to Chow Baseline Harvest
Regression Harvest
C
Control Baseline
Control Regression
Jak2VF Baseline
Jak2VF Regression
D
Lesion Area (µm2)
E
Necrotic Core (µm2)
F
G
Collagen (% of Lesion)
H
DAPI MAC2
I
Macrophage Area (µm2)
Baseline
Regression

696 **Figure 1. Impaired Atherosclerosis Regression in *Jak2^{VF}* CH Mice with Moderate**
697 **Cholesterol Lowering. A.** Study Design. **B.** Plasma cholesterol (n = 34, 55, 55, 54, 16, 16 for
698 Control mice, n=31, 55, 49, 39, 17, 16 for *Jak2^{VF}* mice, for weeks 0, 5, 11, 15, 17.5, 21
699 respectively). **C.** H&E images of aortic root lesions. Black lines, necrotic core. Scale bar, 200
700 µm. **D.** Lesion area, n = 15-23. **E.** Necrotic core area, n = 15-23. **F.** Picrosirius red-stained aortic
701 root lesions. Scale bar, 278 µm **G.** Collagen area as a percentage of lesion area, n = 15-24. **H.**
702 Images of aortic root lesions stained for MAC2 (Green) and DAPI (Blue). Scale bar, 100 µm. **I.**
703 Macrophage area, n = 15-24. All quantifications shown as mean ± s.e.m. Two-way ANOVA with
704 the Geisser-Greenhouse correction for sphericity and Tukey's multiple comparisons test (B).
705 Two-way ANOVA with Tukey's multiple comparisons test (D,E,G,I).

Figure 2

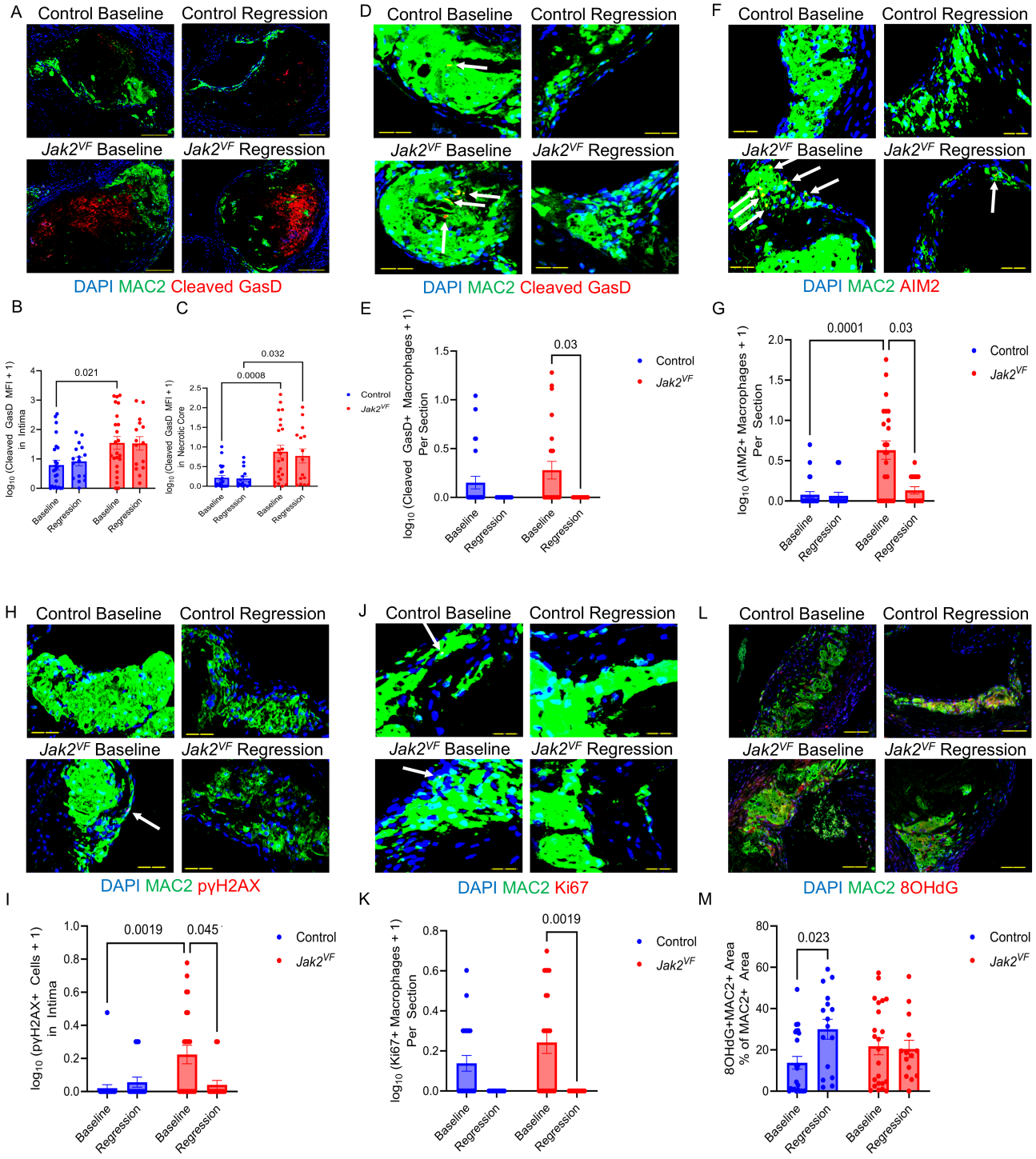
A
Control Baseline
Control Regression
Jak2VF Baseline
Jak2VF Regression
DAPI MAC2 Cleaved GasD
D
Control Baseline
Control Regression
Jak2VF Baseline
Jak2VF Regression
DAPI MAC2 Cleaved GasD
F
Control Baseline
Control Regression
Jak2VF Baseline
Jak2VF Regression
DAPI MAC2 AIM2
B
log10 (Cleaved GasD MFI + 1) in Intima
0.021
Baseline
Regression
Baseline
Regression
C
log10 (Cleaved GasD MFI + 1) in Necrotic Core
0.0008
0.032
Baseline
Regression
Baseline
Regression
Control
Jak2VF
E
log10 (Cleaved GasD+ Macrophages + 1) Per Section
0.03
Baseline
Regression
Baseline
Regression
Control
Jak2VF
G
log10 (AIM2+ Macrophages + 1) Per Section
0.0001
0.03
Baseline
Regression
Baseline
Regression
Control
Jak2VF
H
Control Baseline
Control Regression
Jak2VF Baseline
Jak2VF Regression
DAPI MAC2 pγH2AX
J
Control Baseline
Control Regression
Jak2VF Baseline
Jak2VF Regression
DAPI MAC2 Ki67
L
Control Baseline
Control Regression
Jak2VF Baseline
Jak2VF Regression
DAPI MAC2 8OHdG
I
log10 (pγH2AX+ Cells + 1) in Intima
0.0019
0.045
Baseline
Regression
Baseline
Regression
Control
Jak2VF
K
log10 (Ki67+ Macrophages + 1) Per Section
0.0019
Baseline
Regression
Baseline
Regression
Control
Jak2VF
M
8OHdG+MAC2+ Area % of MAC2+ Area
0.023
Baseline
Regression
Baseline
Regression
Control
Jak2VF

Figure 2. Moderate Cholesterol Lowering Reverses Macrophage AIM2 Inflammasome Activation, DNA Damage, and Proliferation in *Jak2^{VF}* CH Lesions. A. Images of aortic root lesions stained for MAC2 (Green), Cleaved GasD (Red), and DAPI (Blue). Scale bar, 127 µm. **B.** Log_{10} transformed cleaved GasD mean fluorescence intensity (MFI) in lesions with the addition of constant 1, n = 15-24. **C.** Log_{10} transformed cleaved GasD mean fluorescence intensity (MFI) in necrotic cores with the addition of the constant 1, n = 15-24. **D.** Images of aortic root lesions stained for MAC2 (Green), Cleaved GasD (Red), and DAPI (Blue). Scale bar, 40 µm. White arrows, cleaved GasD+ macrophages. **E.** Log_{10} transformed cleaved GasD positive macrophages per section with the addition of constant 1, n = 15-24. **F.** Images of aortic root lesions stained for MAC2 (Green), AIM2 (Red), and DAPI (Blue). Scale bar, 75 µm. White arrows, AIM2 positive macrophages. **G.** Log_{10} transformed AIM2 positive macrophages per section with the addition of constant 1, n = 15-23. **H.** Images of aortic root lesions stained for MAC2 (Green), pγH2AX (Red), and DAPI (Blue). Scale bar, 46 µm. White arrows, pγH2AX positive cells. **I.** Log_{10} transformed pγH2AX positive macrophages per section with the addition of constant 1, n = 15-23. **J.** Images of aortic root lesions stained for MAC2 (Green), Ki67 (Red), and DAPI (Blue). Scale bar, 25 µm. White arrows, Ki67 positive macrophages. **K.** Log_{10} transformed Ki67 positive macrophages per section with the addition of constant 1, n = 15-23. **L.** Images of aortic root lesions stained for MAC2 (Green), 8OHdG (Red), and DAPI (Blue). Scale bar, 78 µm. **M.** Percentage of MAC2 positive area double positive for 8OHdG and MAC2, n = 14-24. MAC2 intensity differences reflect independent staining and imaging sessions across panels. All quantifications shown as mean ± s.e.m. Two-way ANOVA with Tukey's multiple comparisons test (B,C). Kruskal-Wallis test with Dunn's multiple comparisons test (E,G,I,K,M).

729 **Figure 3**

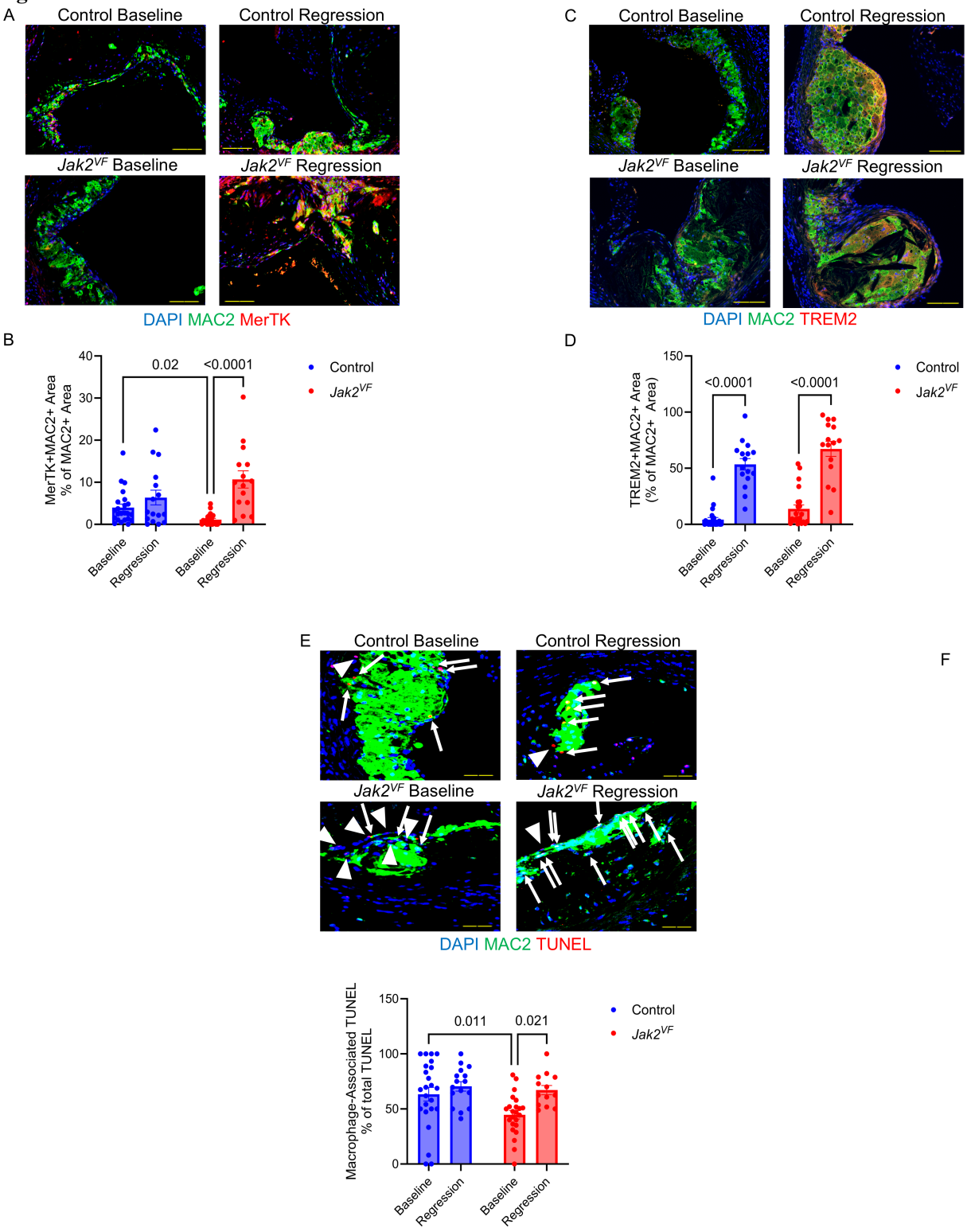
A
Control Baseline
Control Regression
Jak2VF Baseline
Jak2VF Regression
DAPI MAC2 MerTK
B
MerTK+MAC2+ Area
% of MAC2+ Area
0.02
<0.0001
Control
Jak2VF
Baseline
Regression
Baseline
Regression
C
Control Baseline
Control Regression
Jak2VF Baseline
Jak2VF Regression
DAPI MAC2 TREM2
D
TREM2+MAC2+ Area
(% of MAC2+ Area)
<0.0001
<0.0001
Control
Jak2VF
Baseline
Regression
Baseline
Regression
E
Control Baseline
Control Regression
Jak2VF Baseline
Jak2VF Regression
DAPI MAC2 TUNEL
F
Macrophage-Associated TUNEL
% of total TUNEL
0.011
0.021
Control
Jak2VF
Baseline
Regression
Baseline
Regression

730 **Figure 3. Moderate Cholesterol Lowering Reverses Impaired Efferocytosis in *Jak2^{VF}* CH**
731 **Lesions While Increasing TREM2^{Hi} Macrophages in Control and *Jak2^{VF}* CH Lesions A.**
732 Images of aortic root lesions stained for MAC2 (Green), MerTK (Red), and DAPI (Blue). Scale
733 bar, 102 µm. **B.** Percentage of MAC2 positive area double positive for MerTK and MAC2, n =
734 15-23. **C.** Images of aortic root lesions stained for MAC2 (Green), TREM2 (Red), and DAPI
735 (Blue). Scale bar, 100 µm. **D.** Percentage of MAC2 positive area double positive for TREM2 and
736 MAC2, n = 15-24. **E.** Images of in situ efferocytosis in aortic root lesions: MAC2 (Green),
737 TUNEL (Red), and DAPI (Blue). Scale bar, 40 µm. White arrows, nuclei double positive for
738 TUNEL and MAC2. White wedges, nuclei positive for TUNEL but negative for MAC2. **F.**
739 Percentage of TUNEL positive nuclei also positive for MAC2. MAC2 intensity differences
740 reflect independent staining and imaging sessions across panels, n = 13-24. All quantifications
741 shown as mean ± s.e.m. Two-way ANOVA with Tukey's multiple comparisons test (D). Kruskal-
742 Wallis test with Dunn's multiple comparisons test (B,F).

743

Figure 4

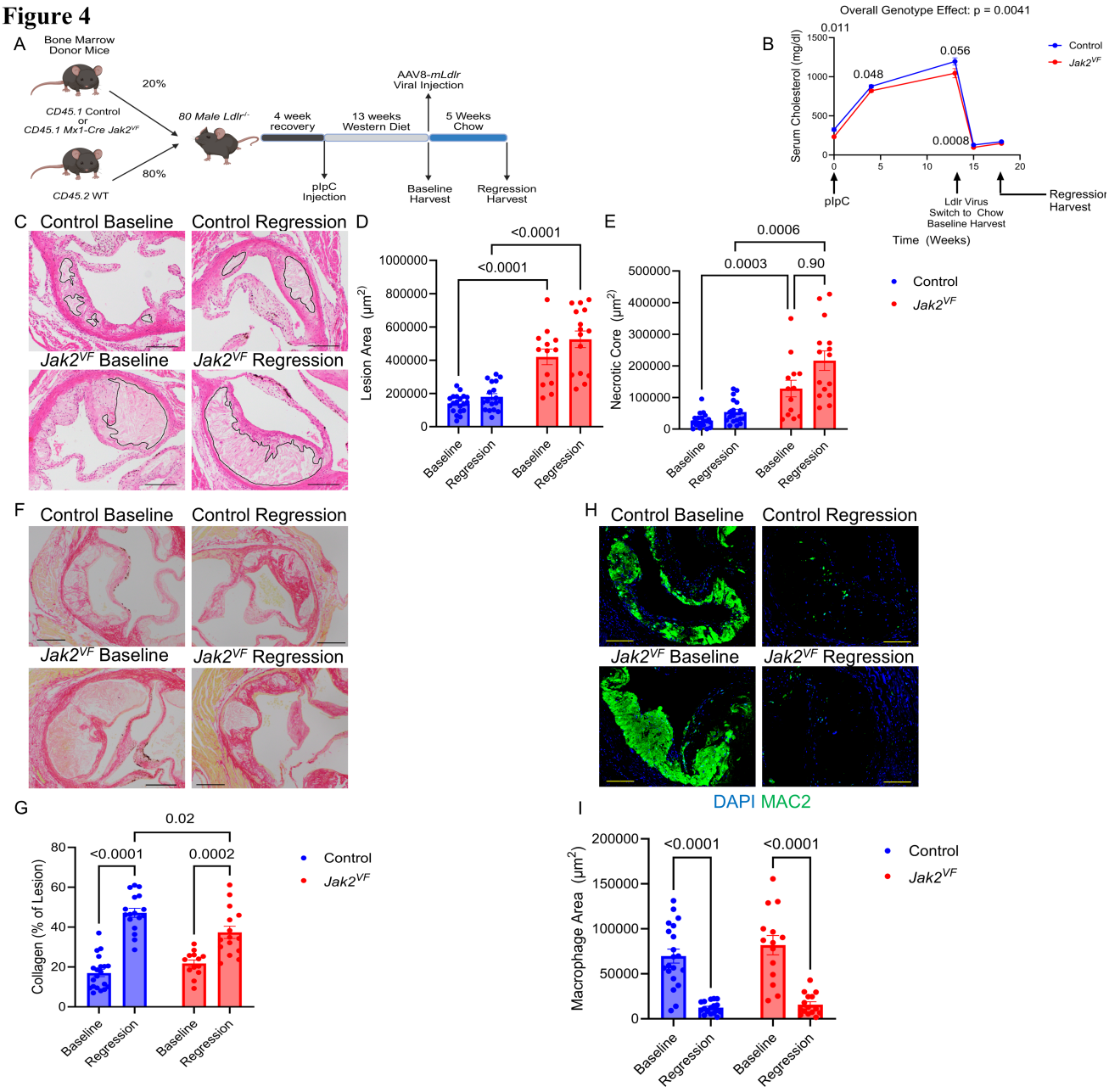
A
Bone Marrow Donor Mice
20%
80%
CD45.1 Control or CD45.1 Mx1-Cre Jak2VF
CD45.2 WT
80 Male Ldlr-/-
4 week recovery
13 weeks Western Diet
AAV8-mLdlr Viral Injection
5 Weeks Chow
pIpC Injection
Baseline Harvest
Regression Harvest
B
Overall Genotype Effect: p = 0.0041
Serum Cholesterol (mg/dl)
0.011
0.048
0.056
0.0008
Control
Jak2VF
pIpC
Ldlr Virus Switch to Chow Baseline Harvest
Regression Harvest
Time (Weeks)
C
Control Baseline
Control Regression
Jak2VF Baseline
Jak2VF Regression
D
Lesion Area (μm2)
<0.0001
<0.0001
Baseline
Regression
E
Necrotic Core (μm2)
0.0006
0.0003
0.90
Control
Jak2VF
F
Control Baseline
Control Regression
Jak2VF Baseline
Jak2VF Regression
H
Control Baseline
Control Regression
Jak2VF Baseline
Jak2VF Regression
DAPI MAC2
G
Collagen (% of Lesion)
0.02
<0.0001
0.0002
Control
Jak2VF
I
Macrophage Area (μm2)
<0.0001
<0.0001
Control
Jak2VF

744 **Figure 4. Aggressive Cholesterol Lowering Normalizes Regression in *Jak2^{VF}* CH Lesions. A.**
745 Study Design. **B.** Plasma cholesterol (n = 5, 38, 19, 18, 18 for Control mice, n = 5, 37, 15, 16, 15
746 for Jak2VF mice, for weeks 0, 4, 13, 15, 18 respectively). **C.** H&E images of aortic root lesions.
747 Black lines, necrotic core. Scale bar, 200 µm. **D.** Lesion area, n = 13-20. **E.** Necrotic core area, n
748 = 13-20. **F.** Picrosirius red-stained aortic root lesions. Scale bar, 219 µm **G.** Collagen area as a
749 percentage of lesion area, n = 13-20. **H.** Images of aortic root lesions stained for MAC2 (Green)
750 and DAPI (Blue). Scale bar, 193 µm. **I.** Macrophage area, n = 13-20. All quantifications shown
751 as mean ± s.e.m. Two-way ANOVA with Tukey's multiple comparisons test (D,G,I). Two-way
752 ANOVA with the Geisser-Greenhouse correction for sphericity and Tukey's multiple
753 comparisons test (B). Kruskal-Wallis test with Dunn's multiple comparisons test (E)

754 **Figure 5**

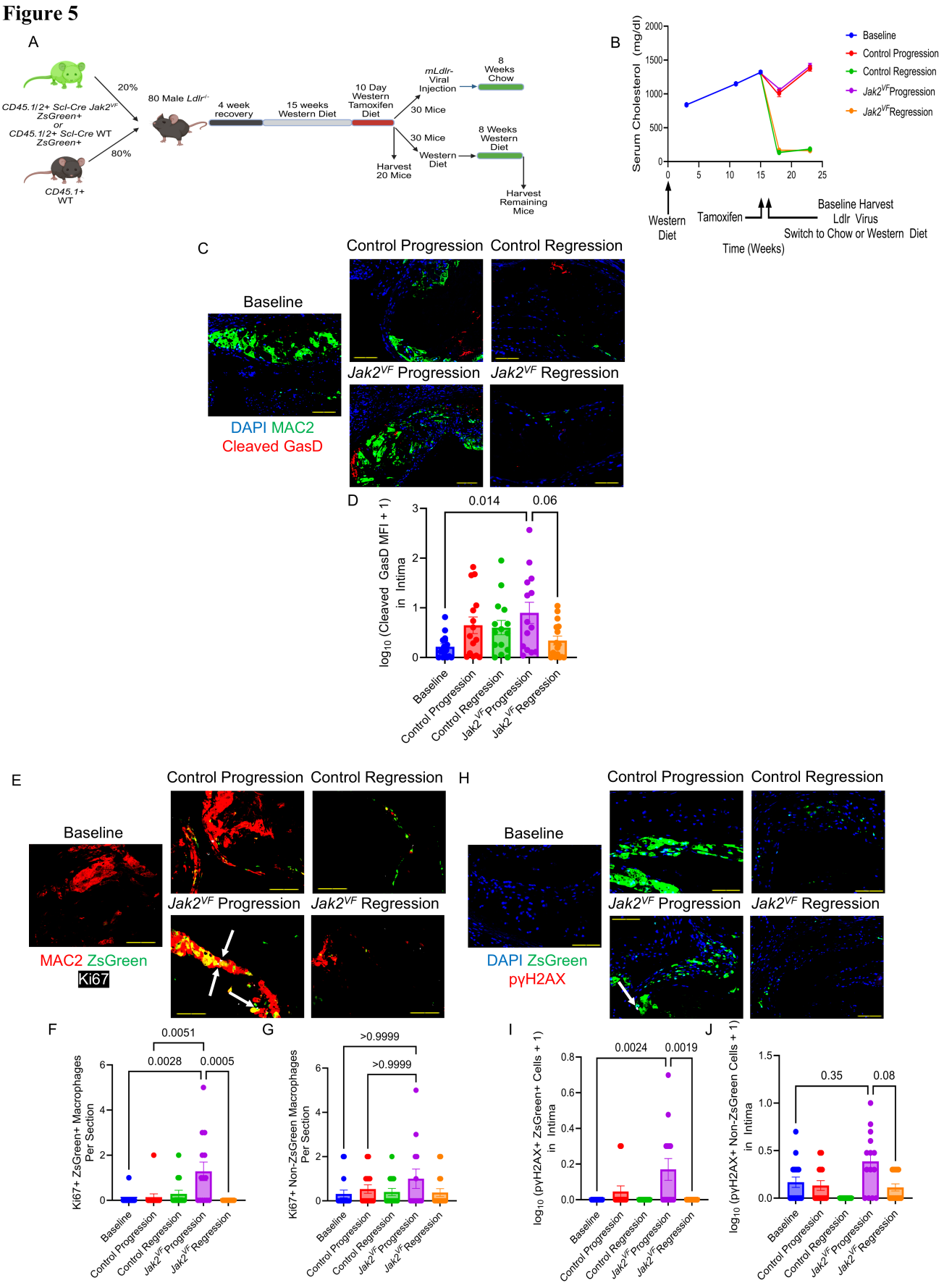
A
CD45.1/2+ Scl-Cre Jak2VF ZsGreen+
or
CD45.1/2+ Scl-Cre WT ZsGreen+
20%
80%
CD45.1+ WT
80 Male Ldlr-/-
4 week recovery
15 weeks Western Diet
10 Day Western Tamoxifen Diet
mLdlr- Viral Injection
8 Weeks Chow
30 Mice
30 Mice
Western Diet
8 Weeks Western Diet
Harvest 20 Mice
Harvest Remaining Mice
B
Serum Cholesterol (mg/dl)
Baseline
Control Progression
Control Regression
Jak2VFProgression
Jak2VFRegression
Western Diet
Tamoxifen
Baseline Harvest
Ldlr Virus
Switch to Chow or Western Diet
Time (Weeks)
C
Control Progression
Control Regression
Baseline
Jak2VF Progression
Jak2VF Regression
DAPI MAC2
Cleaved GasD
D
log10 (Cleaved GasD MFI + 1) in Intima
0.014
0.06
Baseline
Control Progression
Control Regression
Jak2VF Progression
Jak2VF Regression
E
Control Progression
Control Regression
Baseline
Jak2VF Progression
Jak2VF Regression
MAC2 ZsGreen
Ki67
H
Control Progression
Control Regression
Baseline
Jak2VF Progression
Jak2VF Regression
DAPI ZsGreen
pγH2AX
F
Ki67+ ZsGreen+ Macrophages Per Section
0.0051
0.0028
0.0005
G
Ki67+ Non-ZsGreen Macrophages Per Section
>0.9999
>0.9999
I
log10 (pγH2AX+ ZsGreen+ Cells + 1) in Intima
0.0024
0.0019
J
log10 (pγH2AX+ Non-ZsGreen Cells + 1) in Intima
0.35
0.08

755 **Figure 5. Cholesterol Lowering Suppresses *Jak2^{VF}* Macrophage Proliferation and DNA**
756 **Damage. A.** Study design. **B.** Plasma cholesterol (n = 80, 79, 79 for Baseline mice for weeks 3,
757 11, 15 respectively; n = 13, 15 for Control Progression mice, n = 16, 16 for Control Regression
758 mice, n = 15, 15 for *Jak2^{VF}* Progression mice, n = 16, 16 for *Jak2^{VF}* Regression mice, for weeks
759 18, 23 respectively) **C.** Images of aortic root lesions for MAC2 (Green), Cleaved GasD (Red),
760 and DAPI (Blue). Scale bar, 98 µm. **D.** Log_{10} transformed cleaved GasD mean fluorescence
761 intensity (MFI) in lesions with the addition of constant 1, n = 14-16. **E.** Images of aortic root
762 lesions for MAC2 (Red), Ki67 (White), and ZsGreen (Green). Scale bar, 133 µm. White arrows,
763 macrophages double positive for Ki67 and ZsGreen. **F.** Macrophages positive for both Ki67 and
764 ZsGreen per section, n = 14-15. **G.** Macrophages positive for Ki67 but negative for ZsGreen per
765 section, n = 13-16. **H.** Images of aortic root lesions stained for pγH2AX (Red), ZsGreen (Green),
766 and DAPI (Blue). Scale bar, 75 µm. White arrows, pγH2AX positive cells. **I.** Log_{10} transformed
767 cells double positive for pγH2AX and ZsGreen in lesions with the addition of constant 1, n = 13-
768 16. **J.** Log_{10} transformed cells positive for pγH2AX but negative for ZsGreen in lesions with the
769 addition of constant 1, n = 13-16. All quantifications shown as mean ± s.e.m. One-way ANOVA
770 with Holm-Sidak's multiple comparisons test (D). Kruskal-Wallis test with Dunn's multiple
771 comparison's test (F,G,I,J).

772 **Figure 6**

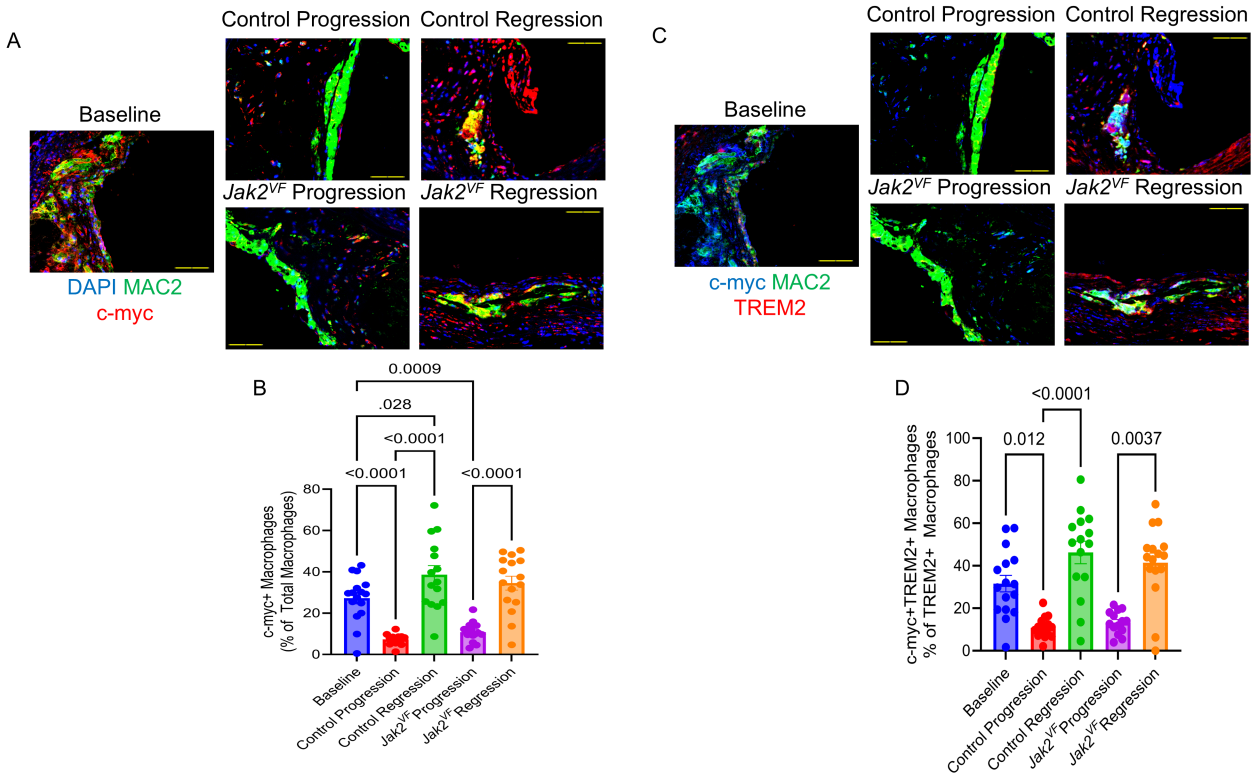
A
Baseline
Control Progression
Control Regression
Jak2VF Progression
Jak2VF Regression
DAPI MAC2
c-myc
B
0.0009
.028
<0.0001
<0.0001
<0.0001
c-myc+ Macrophages
(% of Total Macrophages)
80
60
40
20
0
Baseline
Control Progression
Control Regression
Jak2VF Progression
Jak2VF Regression
C
Baseline
Control Progression
Control Regression
Jak2VF Progression
Jak2VF Regression
c-myc MAC2
TREM2
D
<0.0001
0.012
0.0037
c-myc+TREM2+ Macrophages
% of TREM2+ Macrophages
100
80
60
40
20
0
Baseline
Control Progression
Control Regression
Jak2VF Progression
Jak2VF Regression

773 **Figure 6. Cholesterol Lowering Increases c-myc in TREM2^{Hi} Macrophages. A.** Images of
774 aortic root lesions stained for MAC2 (Green), c-myc (Red), and DAPI (Blue). Scale bar, 121 µm.
775 **B.** Percentage of macrophages positive for c-myc, n = 14-16. **C.** Images of aortic root lesions
776 stained for MAC2 (Green), c-myc (Blue), and TREM2 (Red). Scale bar, 121 µm. **D.** Percentage
777 of TREM2 positive macrophages positive for c-myc, n = 14-16. All quantifications shown as
778 mean ± s.e.m. One-way ANOVA with Holm-Sidak's multiple comparisons test (B). Kruskal-
779 Wallis test with Dunn's multiple comparisons test (D).